Evidence for large lattice relaxation at the *DX* center in Si-doped $Al_xGa_{1-x}As$

P. M. Mooney, G. A. Northrop, T. N. Morgan, and H. G. Grimmeiss*
IBM Thomas J. Watson Research Center, P.O. Box 218, Yorktown Heights, New York 10598
(Received 17 September 1987; revised manuscript received 9 December 1987)

New measurements of the energy dependence of the photoionization cross section of the *DX* center in Si-doped $Al_xGa_{1-x}As$ are reported. With the use of a tunable infrared laser which provides sufficient light intensity in a very narrow wavelength range, the photoionization cross section has been measured over 6–8 orders of magnitude in samples with a variety of alloy compositions and doping concentrations. No measurable signal was observed for photon energies less than 0.8 eV. Data are analyzed in terms of a simple model which gives a value of 1.4–1.8 eV for the photoionization threshold energy. This energy is much larger than the *DX*-center binding energy, confirming that there is a large relaxation of the lattice when charge is captured at the *DX*. The phonon mode involved in the lattice relaxation is found to be 5.5 meV.

INTRODUCTION

The *DX* center is the dominant deep level found in *n*-type $Al_xGa_{1-x}As$ and it is believed to be the cause of persistent photoconductivity observed in this material at low temperature.[1–3] The energy position of this deep level follows that of the conduction-band minimum at the *L* point in the first Brillouin zone and it lies below the bottom of the conduction band for $x > 0.22$.[4,5] The concentration of the *DX* center has usually been found to be equal to the donor concentration in $Al_xGa_{1-x}As$, independent of the conditions or method of epitaxial crystal growth.[6–8] It is observed for all substitutional *n*-type dopants both those on the group-III sites (Ge,Si,Sn) and those on the group-V sites (S,Se,Te). The activation energies for thermal emission and capture vary with the donor species.[9] The emission energy is independent of the alloy composition,[10–12] but the capture energy varies with the crystal band structure.[11–14] The photoionization energy of the *DX* center is much larger than the thermal ionization energy and also varies with the donor species.[1–3,15]

A large-lattice-relaxation (LLR) model for the *DX* center was proposed by Lang *et al.*[1–3] In this model a rearrangement of the atoms surrounding the impurity occurs when an electron is captured at the deep level. This results in a lower total energy than when the electron is in the conduction band. In order to account for the large relaxation of the lattice, it was suggested that the level comes from a complex consisting of the donor atom and an unknown native defect, hence the name *DX* center. Recent measurements of the temperature dependence of the photoionization cross section of the *DX* center in Si-doped $Al_xGa_{1-x}As$ (Ref. 16) support this model and agree well with the earlier data.[15]

Other models for this level have also been proposed. One, which also includes the idea of large lattice relaxation, attributes the level to a donor atom that is displaced from the substitutional site.[17–19] The deep level is proposed to be a bound state of the displaced donor atom associated with the minimum of the conduction band at the *L* point. These authors argue that since the deep-level concentration is independent of the growth conditions, an arsenic vacancy or other native defect cannot be involved. In this model the lattice relaxation results from the displacement of the donor atom when an electron is captured.

A small-lattice-relaxation (SLR) model in which the donor atoms remain at the substitutional site has also been proposed.[20,21] Here the *DX* level is suggested to be a bound state of the substitutional donor atom which is associated with the minimum of the conduction band at the *L* point. This model predicts an optical ionization threshold which is nearly equal to the binding energy of the *DX* level. A low value for the photoionization threshold energy for Si-doped $Al_xGa_{1-x}As$, which supports this model, has recently been reported.[22,23] Another model which attributes the properties of the *DX* center to fluctuations in the band structure due to the random distribution of atoms in the alloy also predicts a photoionization threshold equal to that of the *DX*-level binding energy and data for Sn-doped $Al_xGa_{1-x}As$ were reported in support of this model.[24]

In this paper we report new measurements of the energy dependence of the photoionization cross section. By using a tunable infrared laser which provides sufficient light intensity in a very narrow energy range, we have been able to measure the cross section over as many as 8 orders of magnitude in some cases. We have measured samples with a variety of alloy compositions and doping concentrations and in all cases our data show a value for the threshold energy which is much larger than the *DX*-center binding energy. We conclude that there must be a large lattice relaxation associated with charge capture at the *DX* center. We discuss differences in experimental methods and conditions that might account for the difference between our results and those reported in Refs. 23 and 24.

SAMPLES AND EXPERIMENTAL METHOD

The $Al_xGa_{1-x}As$ layers used for these measurements were grown by molecular-beam epitaxy (MBE). The al-

loy composition of each layer was measured by electron microprobe. Schottky-diode structures were used for the photocapacitance-transient measurements. Three samples with AlAs mole fractions 0.30, 0.48, and 0.74 were grown as follows: a thin buffer layer of GaAs followed by a thin graded layer in which the AlAs mole fraction was increased from zero to the desired value followed by a thick (1 μm) layer of $Al_xGa_{1-x}As$. All of these layers were doped with 7×10^{16} cm^{-3} Si. The layers were grown on *n*-type GaAs substrates, except in the case of the $x=0.30$ sample, which was mistakenly grown on a semi-insulating substrate. 200 Å of Mo was deposited while the samples remained under high vacuum in the MBE chamber to form semitransparent Schottky-barrier diodes. A fourth sample was a modulation-doped field-effect transistor (MODFET) with a 500-Å-thick $Al_xGa_{1-x}As$ layer doped with 1×10^{18} cm^{-3} Si and with $x=0.27$. The Schottky gate was made by depositing Ti/Pt/Au. Ohmic contacts on all of these samples were standard AuGe/Ni/Au alloy contacts. In the case of the MODFET and the $x=0.30$ sample the Ohmic contacts were made on the top surface of the $Al_xGa_{1-x}As$ layer. When a conducting substrate was used, Ohmic contact was made to the substrate. These samples were similar to the two series of samples used for the photoionization cross-section measurements reported in Ref. 16. Thermal emission and capture measurements for the *DX* center in these samples have been reported.[11–14] A sample for photoconductivity transients was also prepared from the thick $Al_xGa_{1-x}As$ layer ($x=0.30$) grown on the semi-insulating substrate. After removing the thin Mo layer from the surface, Ohmic contacts were made by alloying Sn balls onto the $Al_xGa_{1-x}As$ layer. No photovoltaic effect or rectification was observed. When the sample was cooled in the dark the resistance was high, indicating that the Ohmic contacts were shallow enough not to contact the underlying GaAs layer.

Samples were mounted in a liquid-nitrogen cryostat having a sapphire window. The transmission of the window was measured to be 90% out to a wavelength of 2600 nm. During the measurements the samples were held at a constant temperature of 82 K, measured with a copper-Constantan thermocouple placed on the header adjacent to the sample.

Two different monochromatic light sources were used for these experiments. A quartz halogen lamp with narrow-band interference filters was used in the wavelength range of 650–2300 nm. For $650\leq\lambda\leq1200$ nm, the bandwidth $\Delta\lambda$ was 10 nm. For $\lambda=1300$, 1400, and 1500 nm, $\Delta\lambda=40$ nm. For $\lambda\geq1600$ nm, $\Delta\lambda=60-80$ nm. A lens focused the light onto the sample. The filter holder and shutter were mounted on the window of the cryostat so as to prevent stray light from striking the sample. Calibrated neutral-density filters were placed in front of the interference filter to reduce the light intensity when necessary. The transmitted power at each wavelength was measured by placing a thermopile in place of the sample. The area of the focal spot, which was considerably larger than the area of the samples, was measured in order to determine the photon flux incident on the sample.

The second light source, a laser, was an optical parametric oscillator (OPO) which produces a continuously tunable, well-collimated beam over the spectral range 900–1600 nm, with a linewidth of less than 1 nm.[25] The system involves a 20-W copper-vapor laser pumping a grating tuned dye laser–amplifier circulating Kiton red or Rhodamine-6G dye. The dye laser, in turn, pumps the OPO, which consists of a 5-cm-long *c*-axis $LiNbO_3$ crystal in an oscillator configuration. Nonlinear mixing in the crystal splits a dye photon into two infrared photons, in an energy ratio determined by a phase-matching condition. The infrared wavelengths are tuned by variation of either the dye wavelength or the crystal temperature. The desired infrared wavelength is then isolated and measured by a pass through a grating monochromator, resulting in usable narrow-band powers in the (5–30)-mW range.

As shown in Fig. 1, the beam was then focused onto an 0.6-mm aperture, after which it was split into a reference beam and a sample beam. These beams passed through lenses which image the aperture 1:1 onto a Ge photodiode and the sample, respectively. The reference beam is chopped, and the reference signal detected synchronously. When calibrated by replacing the sample with a thermopile, the reference beam provided a measure of the power at the sample with a dynamic range of 10^5 or better. The variable attenuator allowed continuous adjustment of the power by a factor of 10^4 to obtain a measurable transient over the wide range of cross sections encountered. This *in situ* measurement of the power was required by the variability of the laser power as compared to the lamp source.

Optical emission transients of the Schottky-diode samples were measured using a capacitance feedback circuit to maintain a constant capacitance and measuring the voltage applied to the diode as a function of time. This technique keeps the depletion depth constant, thus avoiding nonexponential transients due to the large trap concentrations in these samples.[2] The sample was cooled to the measurement temperature at zero bias to establish an

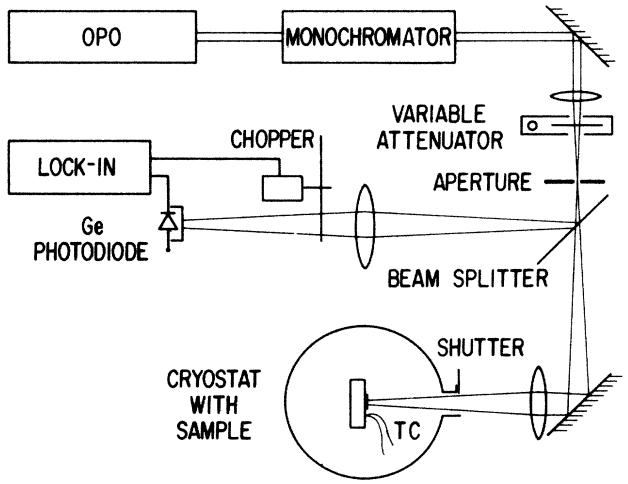

FIG. 1. Schematic diagram of the optical system for the infrared-laser-light source.

initial condition with all of the *DX* centers occupied (neutral). For some samples all of the electrons in the undepleted part of the layer become trapped at *DX* centers and the material contains almost no free carriers. This results in a flat *C-V* curve for negative voltages applied to the Schottky contact, such as curve (*a*) in Fig. 2. Thus it is not possible to choose a suitable value for the capacitance. Since the photoionization is persistent at these temperatures, i.e., there is a barrier which prevents the electrons in the conduction band from being trapped at the *DX* centers, we initialized the sample by exposing the sample to light with no applied voltage until the desired value of the capacitance was reached. After this the *C-V* curve, which is stable, was like curve (*b*) in Fig. 2. A suitable value of the capacitance was then chosen (this value was slightly smaller than the value at 0 V after initialization as shown in Fig. 2) and the voltage transient at constant capacitance was measured. At the completion of the photoionization process the *C-V* curve was like curve (*c*) in Fig. 2.

Full photocapacitance transients were measured at various wavelengths. They were found to be exponential in form and the amplitude was the same for all wavelengths of incident light out to 1220 nm, as was reported in Ref. 16. The photoionization cross section was calculated using the equation $\sigma_n^0(h\nu)=(\phi\tau)^{-1}$, where τ is the time constant of the emission transient and ϕ is the photon flux at the sample surface. At a wavelength of 1050 nm the time required to measure the full transient was the order of an hour and it increased by orders of magnitude as the wavelength was increased. Therefore, to get data in a reasonable amount of time the initial slope of the voltage transient was used to determine the photoionization cross section.

At very short times an exponential transient of the form $V(t)=\Delta V(1-e^{-t/\tau})$ is linear in time. The voltage signal was amplified by 10^3 and a voltage change of less than 0.3% of ΔV measured. The variation in the initial slope of the first transient after the sample was initialized under the same conditions was a factor of 3. We found that the difference in initial slope between the largest and smallest of 10 transients taken successively without reinitializing the sample was a factor of 1.5, about half of the error to initialize the sample. Therefore up to 10 transients were measured for each initialization. We estimate the uncertainty in the cross sections taken from the initial slopes to be equal to the uncertainty resulting from the initialization procedure, a factor of 3. Figure 3 shows the photon-energy dependence of the photoionization cross section calculated from measurements of both full transients and initial slopes for the same sample. The results agree within the uncertainty of the measurements.

The procedure for collecting the data was to adjust the light intensity to give a transient with the fastest initial slope which could be measured. As the wavelength was increased, it was necessary to increase the light intensity in order to have the same initial slope. Once the intensity was at a maximum, the slopes were measured for longer and longer times, but always for the same voltage change. Figure 4 demonstrates that the initial slope of the photocapacitance transients varies linearly with the light intensity at a fixed energy over the range of slopes we were able to measure.

The photoconductivity transients were taken by using a constant-current source and measuring the voltage drop across the sample as a function of time. The sample was

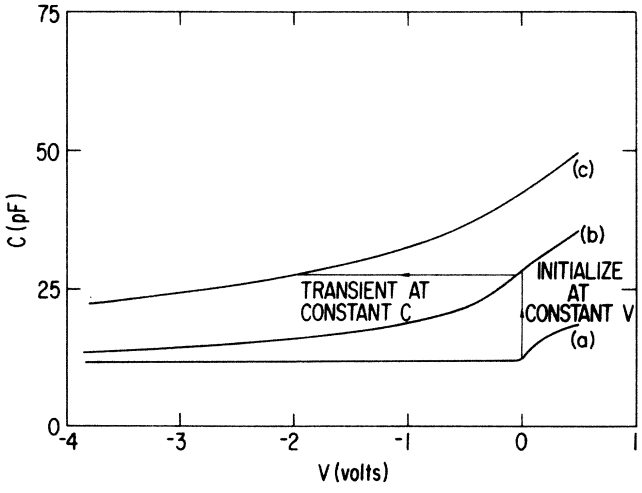

FIG. 2. *C-V* curves showing the method of initializing the samples and measuring the photocapacitance transients for the Schottky diodes.

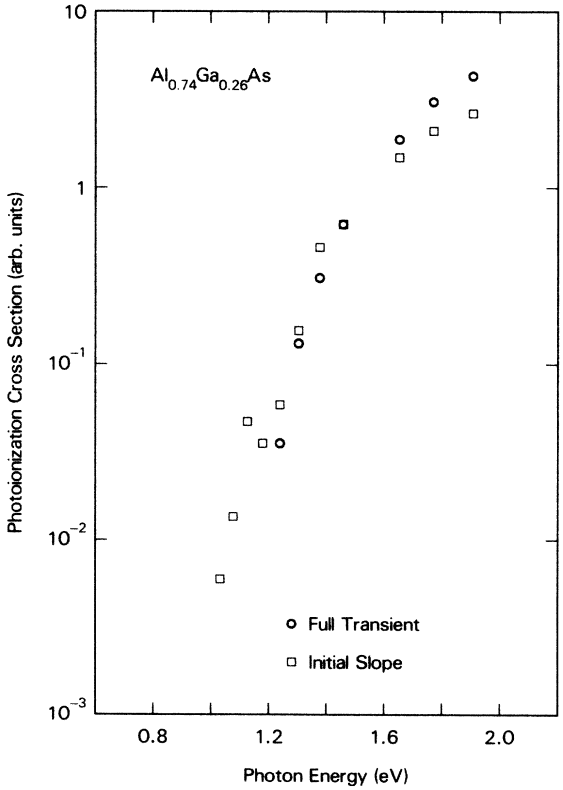

FIG. 3. Photoionization cross section for a Schottky diode with $x=0.74$. Data were calculated from both full transients and initial slopes at each photon energy.

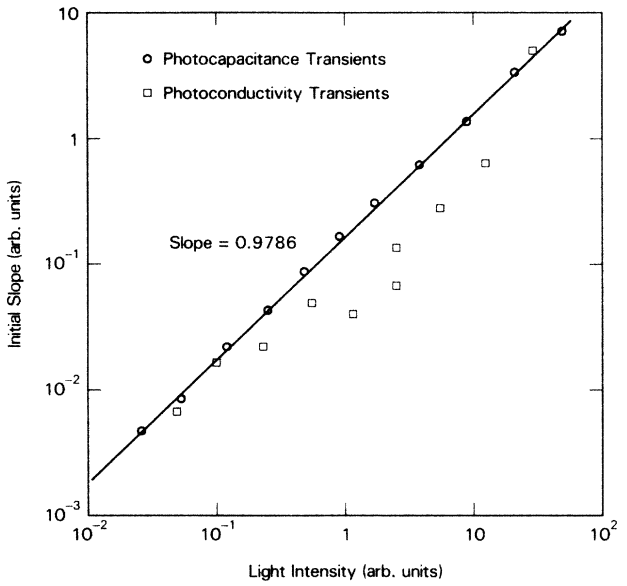

FIG. 4. The dependence of the initial slope of the photocapacitance transients and photoconductivity transients on the laser-beam intensity.

cooled to the measurement temperature with no current passing through it. The initial slopes of the photoconductivity transients were measured by the same procedure as for the photocapacitance transients. Measurements of the full transients at some wavelengths show that they are exponential. Though the magnitude seems to decrease with increasing wavelength, the change in amplitude is less than a factor of 2 at the longest wavelength measured (1400 nm).

RESULTS AND DISCUSSION

The results of our measurements on four samples are shown in Fig. 5. Data taken with both light sources are plotted together for each sample. In all cases there is a smooth decrease of the photoionization cross section as the photon energy decreases and the shape of the curve shows that a transition from a bound state to a band is observed. The sign of the photocapacitance signal indicates that an electron from the *DX* center is ionized to the conduction band. Comparison of the photocapacitance data for the three samples in Figs. 5(a)–5(c), which have similar doping concentrations, but different alloy compositions, shows that there is very little variation of σ_n^o with alloy composition. A comparison of the photocapacitance data in Figs. 5(c) and 5(d) for samples with similar alloy compositions but different Si concentrations shows that there is no dependence on the *DX*-center concentration either.

Figure 5(c) shows the spectral distribution of the photoionization cross section obtained from measurements of both the photocapacitance transients and photoconductivity transients on samples prepared from the same wafer. While the data show the same general shape, a direct comparison of the two spectral distributions is difficult to perform since, in general, photoconductivity measurements do not provide absolute values of photoionization cross sections.[26] In order to correlate the two distributions, a few assumptions have therefore to be made which, as will be shown, are supported by the experimental results.

To make the analysis more transparent, it may be useful to examine the two types of measurements in detail. In the photocapacitance samples the *DX* centers that are ionized by the incident photons are in the depletion region of a Schottky diode. When the electron reaches the conduction band it is immediately swept out of the depletion region by the electric field and there is negligible probability that it can be recaptured at the *DX* center. The linear relation between the initial slope of the photocapacitance transient and the light intensity shown in Fig. 4 confirms that recapture of an electron can be neglected in these measurements. Thus only one dominant process is possible in this type of sample, that of electron emission from the *DX* center. The voltage required to have a depletion region of a specified width is determined by the net ionized charge in the depletion region. Since other processes can be neglected, the rate of change of this voltage must be the ionization rate of the *DX* center. In this type of sample one worries about the effect of the electric field on the emission process. Any enhancement of the emission process by tunneling due to the electric field would result in a faster photocapacitance transient and larger value for σ_n^o at the lower photon energies.

For the photoconductivity measurements a constant current flows laterally through the $Al_xGa_{1-x}As$ layer between two Ohmic contacts. Thus there are always free electrons in the conduction band in the region of the ionized deep levels and there is the possibility of recapture of an electron. In the case of the *DX* center, however, the thermal capture cross section is temperature dependent and is quite small at low temperatures, 10^{-26} cm^2 or smaller, depending on the alloy composition of the $Al_xGa_{1-x}As$ layer. Consequently, this capture process is expected to be negligible and both photocapacitance and photoconductivity measurements might be expected to give the same result. From the data in Fig. 4 it is quite clear that the initial slope of the photoconductivity transients does not vary linearly with the light intensity at a fixed energy. This nonlinear behavior suggests that recombination probably cannot be neglected. If the capture process is not negligible, it causes a reduction of the rate at which the free-carrier concentration increases and would result in a smaller value of the photoionization cross section than the true value. Since capture is probably favored at higher photon energies where the excited electrons have a greater chance to return to the *DX* center before thermalization than at small photon energies, we chose to normalize the two spectral distributions in Fig. 5(c) at small photon energies. The deviation of the two spectral distributions at higher photon energies may then be caused partly by the electric field in the diodes and partly by recombination processes in the photoconductivity sample.

In order to determine the absolute value of the photoionization cross section, we have measured the reflectivity of one of the samples with semitransparent

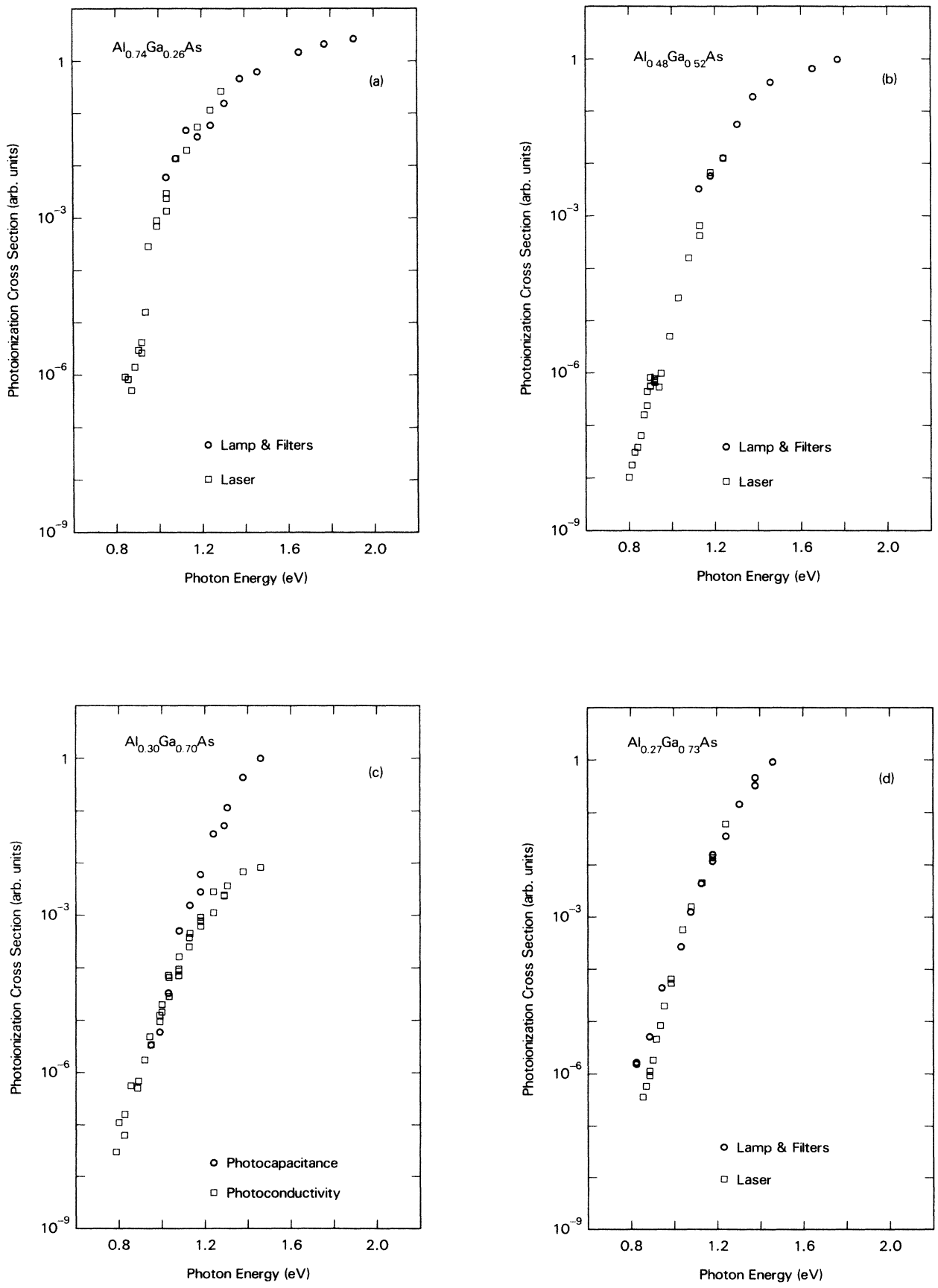

FIG. 5. Photoionization cross sections for four samples of $Al_xGa_{1-x}As$. The samples with $x=0.74$, 0.48, and 0.30 have a Si-doping concentration of 7×10^{16} cm^{-3}. The $x=0.27$ sample has a Si-doping concentration of 1×10^{18} cm^{-3}.

Schottky contacts. A large piece of the $x=0.30$ wafer was used and 53% of the incident light was found to be reflected independent of the wavelength of the incident light. Having determined the photon flux incident on the sample for the halogen lamp with the filters, the absolute value of the cross section was determined from the measurements of the full transients for the $x=0.30$ and 0.74 samples. The data for these samples are plotted on an absolute scale in Fig. 6. Note that the value for the cross section is about an order of magnitude smaller than for other deep levels.[27]

Recently, other data for the energy dependence of the photoionization cross section of the *DX* center in Si-doped $Al_xGa_{1-x}As$ measured from photoconductivity transients have been reported.[21–23] The magnitude of the maximum value of the photoionization cross section was about 2 orders of magnitude higher than we report here. Data for a sample with an alloy composition $x=0.33$ and a Si-doping concentration of about 1×10^{17} cm^{-3} showed structure and a much lower threshold energy than both the photocapacitance and photoconductivity data reported here for a similar sample ($x=0.30$). A difference in the threshold between lightly and heavily doped samples was also reported.[21] Both the structure and the lower threshold energy of the spectral distribution was observed at values of the relative photoionization cross section much smaller than had been previously measured.[16] It was therefore argued that this was one of the reasons why such a structure was not observed in previous studies.

There is also a discrepancy in the reported values of the photoionization cross section for the *DX* center in Sn-doped $Al_xGa_{1-x}As$. Measurements using photocapacitance transients show a decrease of more than 4 orders of magnitude in $\sigma_n^o(h\nu)$ when the photon energy is decreased from 1.46 to 0.8 eV.[15] On the other hand, data from photoconductivity transients shows an increase of about an order of magnitude in $\sigma_n^o(h\nu)$ for the same range of photon energies and then a decrease of 5 orders of magnitude, but with no structure, when the photon energy was decreased further.[24]

Since photoconductivity measurements, in general, do not reflect the spectral distribution of photoionization cross sections,[26] we increased the sensitivity of our photocapacitance method to investigate whether or not such a structure exists at the low-energy tail of the optical distribution. We found no difference between lightly and heavily doped samples. We observed no structure in the spectral distribution of the photoionization cross section and none of our samples gave a measurable signal for photon energies less than 0.8 eV. Therefore, the implication is that the photoconductivity transients observed for photon energies less than 0.8 eV originate from some other deep level which is present in those samples, and not the *DX* center.

In order to test this hypothesis, we performed measurements of the photoionization cross section on a sample identical to that measured in Ref. 23. The Schottky diodes were prepared in our laboratory using the same techniques as for our samples. The results are shown in Fig. 7 along with the data for our sample with a similar

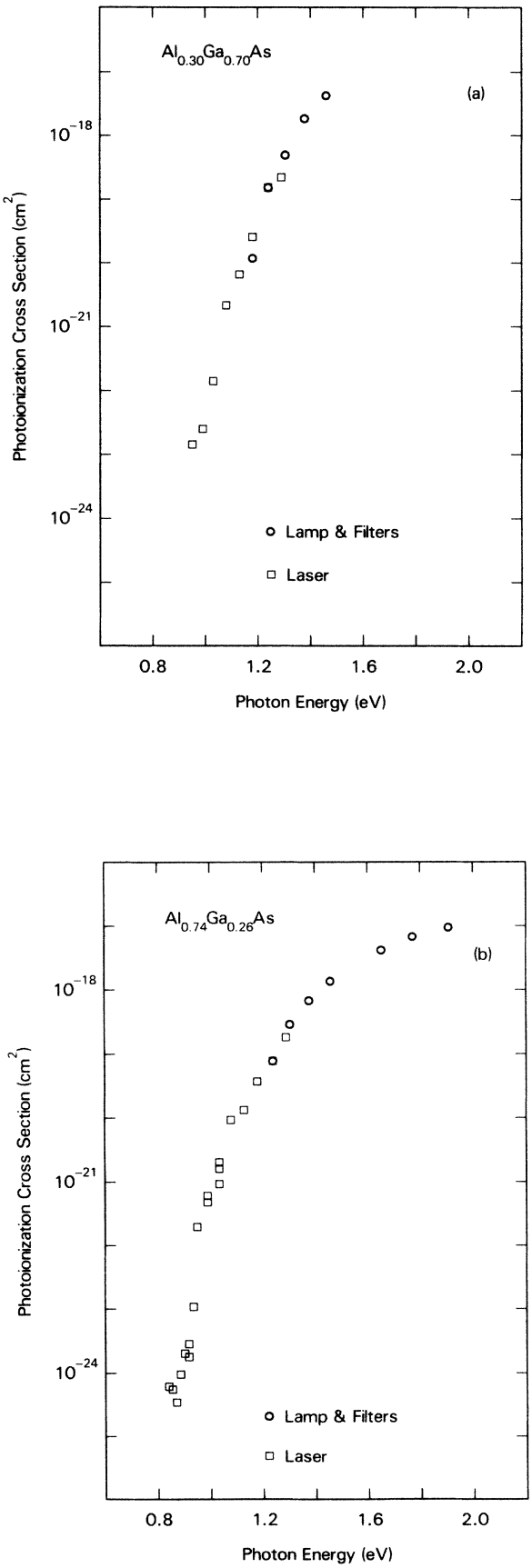

FIG. 6. Absolute value of the photoionization cross sections for samples with $x=0.30$ and 0.74.

composition. There is excellent agreement between the two samples, except for a peak in $\sigma_n^0(h\nu)$ at about 1 eV. Deep-level transient-spectroscopy (DLTS) measurements show that there are two additional electron traps in this sample: one with thermal activation energy 0.69 eV at a concentration of 1.9×10^{-15} cm^{-3}, and another with a thermal activation energy of 1.03 eV at a concentration of 7.5×10^{-14} cm^{-3}. It seems likely that the peak in the energy spectrum of the photoionization cross section is due to the latter trap.

In order to deduce some physical parameters from the data, we employ the simplest model that is consistent with the known properties of *DX* centers. We sketch this model below and give more details in the Appendix. We assume that the deep state is formed from a donor associated with one L valley of the conduction band and perturbed by a potential which varies with a single lattice-distortion coordinate, Q.[28] Thus, we write the effective-mass Hamiltonian,

$$H=-\nabla^2-2/r+H_1(Q)+H_{\rm el}(Q)\ , \tag{1}$$

where the units are the effective Rydberg, Ry*, and Bohr radius, a_0^*, in an L valley, and the last two terms are the unperturbed Hamiltonian and the electron-lattice coupling for the mode represented by Q. We seek the adiabatic potentials $E_L(Q)$ for the L-band edge and $E_0(Q)$ for the lowest bound state generated by this Hamiltonian. These curves define the configuration-coordinate (CC) diagram of the system. We have employed an approximate Green's-function method to calculate $E_0(Q)$, as there is no simple analytic function to describe it.[29]

We find that even linear coupling, $H_{\rm el}=-\alpha Q v(r)$, causes nonlinear changes in the adiabatic potential $E_0(Q)$,[30] and in a system which has a large lattice relaxation the CC curves are even more complex. This is because the dominant phonon modes themselves change as the binding energy increases and the wave function becomes more localized, making the effective electron-lattice coupling highly nonlinear. This is illustrated in Fig. 8, which shows a simplified CC diagram for a ($1s$) Coulomb state perturbed by a local (one-band, one-site) potential of strength approximately proportional to Q.[31] Had the lattice relaxation been treated self-consistently, the potential barrier between $Q=0$ and $Q=Q_0$ would have been even higher. Because of this complexity, it is unproductive to attempt a fit to a set of simple parabolic CC curves, and we must make changes in the usual fitting procedure and its interpretation.

We use the fact that the important optical processes occur near the point $Q=Q_0$ at the minimum of the lower potential curve, and that in this region the dominant phonon mode[32] is reasonably well defined. We then construct a fictitious CC diagram, as in Fig. 8, which ignores the fact that a self-consistent solution would involve different modes away from Q_0, and base our solution on the following assumptions.

(1) Both potential curves are parabolic near their minima, though their curvatures may be different. We denote the phonon energy in the upper parabola by $\hbar\omega_L$ and that near the minimum of the lower curve by $\hbar\omega_0$. Hence, the probability distribution in Q space for the initial states is described by a Gaussian having a variance

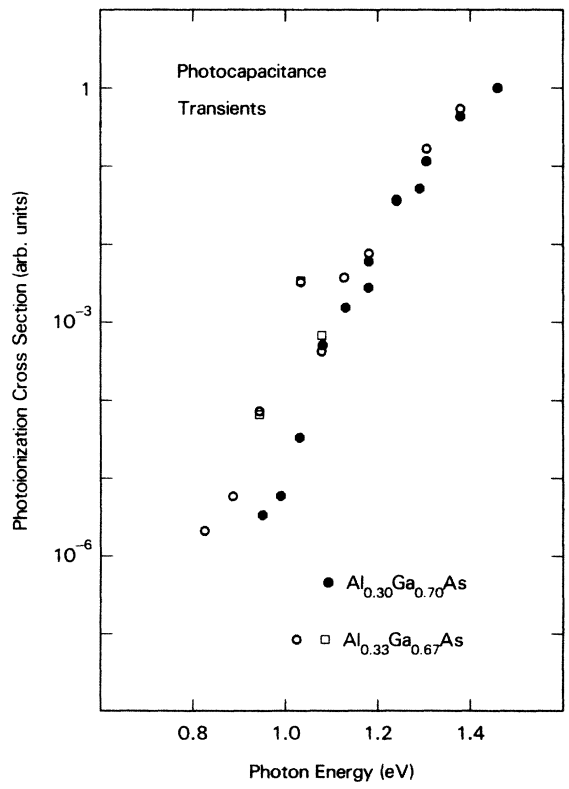

FIG. 7. Comparison of the photoionization cross section for our $x=0.30$ sample with one having $x=0.33$ identical with the sample measured in Ref. 23.

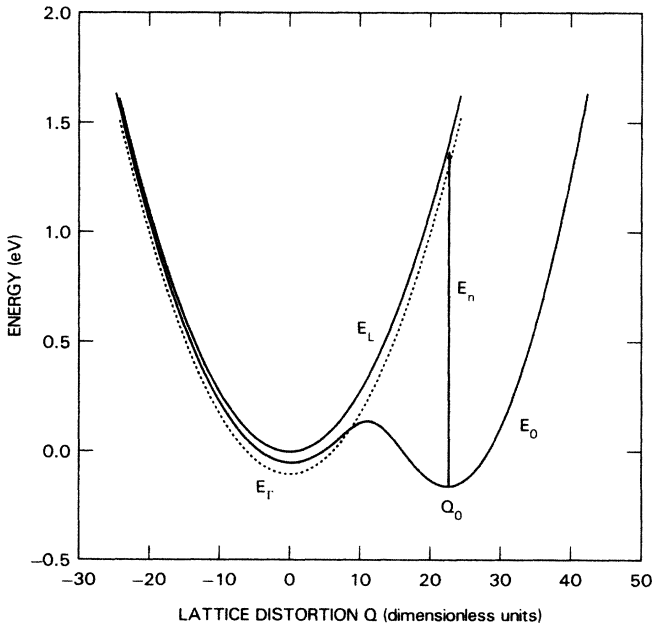

FIG. 8. Possible CC diagram for a deep Coulomb state derived from conduction band at the L point. The conduction-band at the Γ point is also shown for $x\sim0.30$. The effective-mass Rydberg is Ry* = 50 meV, the phonon energy is $\hbar\omega_L=5.5$ meV, and the Huang-Rhys factor is 260.

$$\sigma_Q^2 = \tfrac{1}{2}\beta_0^{-2}\coth(\hbar\omega_0/2k_BT) , \quad (2)$$

where the factor β_0 is defined in Ref. 28.

(2) The optical transitions are vertical in Q space, the Franck-Condon principle, so that the Q-space broadening is converted into an energy broadening according to the slope of the energy difference near $Q=Q_0$,

$$\frac{d(E_L-E_0)}{dQ} = K_L Q_0 ,$$

where K_L is the stiffness coefficient for the distortion. Thus, we find that the variance in energy is given by

$$\sigma_E^2 = (K_L Q_0)^2 \sigma_Q^2 = S(\hbar\omega_L)^2(\omega_L/\omega_0)\coth(\hbar\omega_0/2k_BT) , \quad (3)$$

where S is the Huang-Rhys factor, so that $S\hbar\omega_L$ is the Franck-Condon energy.[33]

(3) The optical transition rate into states at an energy δE above the L-band edge is given, for small δE, by the product of the density of states and the square of the optical matrix element.

$$W(h\nu) \propto (\delta E)^{3/2}/(h\nu)^2 . \quad (4)$$

This is equivalent to Eq. (11) of Ref. 2 with only the first term in the square matrix element factor retained.

With these assumptions the photoionization cross section, σ_n^o, for photon energy $h\nu$ is the convolution of the transition rate, Eq. (4), with the Gaussian distribution of initial Q values and can be written as

$$\sigma_n^o \propto [\sigma_E^{3/2}/(h\nu)^2]y(z) , \quad (5)$$

where the function $y(z)$ is defined in the Appendix and $z=E_n/\sigma_E$ with $E_n \equiv E_L(Q_0)-E_0(Q_0)$. We have integrated Eq. (A2), tabulated the function $y(z)$, and used it to find the two parameters E_n and σ_E, which give the best fit to the photoionization cross-section data. The results appear in Table I. An example of such a fit is shown in Fig. 9 for the sample with $x=0.27$. A similar fit to the temperature dependence of the cross section at fixed photon energy from Fig. 4 of Ref. 16 was made and is shown in Fig. 10. This latter sample, with $x=0.33$, gave the values $E_n=1.189$ eV and $\hbar\omega_0=5.53$ meV.

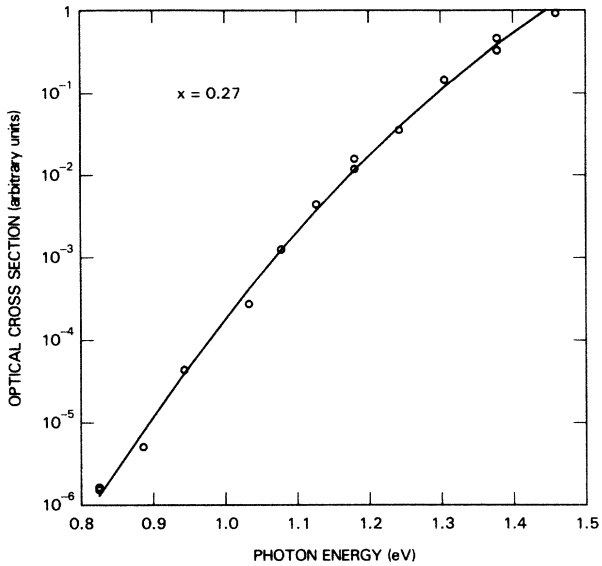

FIG. 9. Fit to the photoionization cross-section spectrum for the $x=0.27$ sample. The data are those of Fig. 5(d) taken with the lamp plus filters.

Because of the limited energy range available and the scatter in the data, the parameters in Table I cannot be fixed with precision, although some trends can be identified. There seems to be a small decrease in the threshold energy as the Al mole fraction of the $Al_xGa_{1-x}As$ layer increases. Such an increase was not observed by Legros *et al.*[16] and it may occur here because the energy range of the data increases as the band gap increases. The threshold energy found here is a bit larger than that reported by Legros *et al.*[16] This could be due to the difference in the equation used to fit the data or to the smaller energy range of the data in Ref. 16. What is clear from these measurements is that the threshold energy for the optical ionization of the *DX* center is about *10 times larger* than the thermal binding energy

TABLE I. Fitting parameters E_n and σ_E for the photoionization cross-section spectra. The data sets 1–4 are data from photocapacitance-transient measurements and data set 3C is from photoconductivity-transient measurements. The "error" is the rms difference in the natural logarithms of the data and the fitted curves. The last column is obtained from Eq. (A3).

Data	AlAs mole fraction	E_n (eV)	σ_E (eV)	Error	$\hbar\omega_L$ (meV)
1 (filters)	0.74	1.39	0.165	0.29	6.6
2 (filters)	0.48	1.37	0.118	0.28	5.0
2 (laser)	0.48	1.43	0.119	0.57	4.7
3 (filters)	0.30	1.67	0.144	0.40	5.2
3 (laser)	0.30	1.89	0.162	0.46	5.5
3C (filters)	0.30	1.74	0.186	0.58	6.6
3C (laser)	0.30	1.48	0.142	0.38	5.5
4 (filters)	0.27	1.72	0.171	0.23	6.1
4 (laser)	0.27	1.81	0.156	0.29	5.2

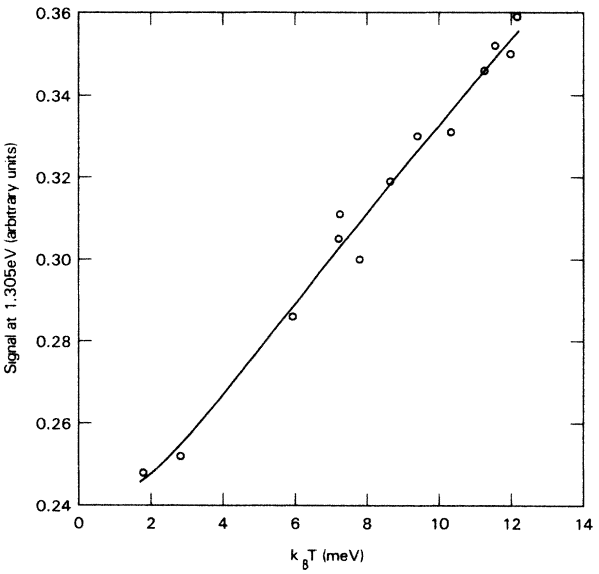

FIG. 10. Fit to the temperature dependence of the photoionization cross section for $h\nu = 1.305$ eV. The data are from Fig. 4 of Ref. 16. The fitting parameters are $E_n = 1.189$ eV and $\hbar\omega_0 = 5.53$ meV.

E_B, which is near 160 meV. Thus there must be a large relaxation of the lattice when an electron is trapped at this deep level.

The data in the last column of Table I are found by equating the values found for σ_E to the expression in Eq. (A3) assuming the value $\hbar\omega_0 = 5.5$ meV, from Fig. 10. All of the phonon energies are found to lie near $\hbar\omega_L = 6$ meV. The small value of these energies is consistent with results in Refs. 2 and 16, where a large-lattice-relaxation model was also used to analyze the photoionization spectra. These results are completely different from those reported by Henning and Ansems,[21-23] who not only find a much lower value for the photoionization threshold energy, but also deduce from photoluminescence data that the phonon mode is 48 meV. This discrepancy suggests that they are observing some other process not involving the *DX* center in the photoluminescence experiments.

CONCLUSIONS

We have presented new data demonstrating that the photoionization cross section of the *DX* center in Si-doped $Al_xGa_{1-x}As$ is essentially independent of both the alloy composition and the Si concentration. More importantly, we have measured the photoionization cross section over 6–8 orders of magnitude and have observed no measurable signal below 0.8 eV. We show that the threshold for optical ionization is *much larger* than the binding energy of the *DX* center. Consequently, a large lattice relaxation must accompany the capture of an electron at this deep level. We also show that a 6-meV phonon mode is involved in the lattice-relaxation process.

ACKNOWLEDGMENTS

Samples for these experiments were provided by M. Heiblum and S. L. Wright. This work was partially supported by the U.S. Office of Naval Research under Contract No. N00014-85-C-0868. One of us (H.G.G.) would like to thank the IBM Corporation for supporting his stay at the Thomas J. Watson Research Center, Yorktown Heights, NY. We are grateful to J. C. M. Henning for giving us a sample identical to the one he measured in Ref. 23.

APPENDIX

The photoionization cross section, σ_n^o, is the convolution of the transition rate, Eq. (4), with the Gaussian distribution of transition energies. This leads directly to Eq. (5) with

$$y(z) \equiv \int_0^\infty dx\, x^{3/2} \exp[-(x-z)^2/2] , \tag{A1}$$

where $x = \delta E/\sigma_E$ and $z = (h\nu - E_n)/\sigma_E$. The integral in Eq. (A1) is related to a parabolic cylinder function,[34]

$$y(z) = (3\sqrt{\pi}/4)\exp(-z^2/4) D_{-5/2}(-z) ,$$

and satisfies the differential equation

$$y'' + zy' - 3y/2 = 0 . \tag{A2}$$

The fitting procedure allows us to determine the variance, σ_E^2, in energy of the photoionization spectrum and the central energy E_n. To determine the other parameters we need to know the binding energy E_B, which is the difference between E_n and the Franck-Condon energy $S\hbar\omega_L$ and one of the phonon energies. We take these to be $E_B = 160$ meV from the published hall data[5] and $\hbar\omega_0 = 5.5$ meV, from the fit in Fig. 9. By combining these values with the values of σ_E given in Table I and using Eq. (3), we obtain

$$\hbar\omega_L = \left[\frac{\sigma_E^2 \hbar\omega_0}{E_n - E_B} \tanh\left(\frac{\hbar\omega_0}{2k_B T} \right) \right]^{1/2} \tag{A3}$$

and the values for $\hbar\omega_L$ shown in the last column of the table.

*Permanent address: Department of Solid State Physics, University of Lund, P.O. Box 118, S-221 00 Lund, Sweden.

[1] D. V. Lang and R. A. Logan, Phys. Rev. Lett. **39**, 635 (1977).
[2] D. V. Lang, R. A. Logan, and M. Jaros, Phys. Rev. B **19**, 1015 (1979).
[3] D. V. Lang, in *Deep Centers in Semiconductors*, edited by S. T. Pantelides (Gordon and Breach, New York, 1986), pp. 489–539.
[4] A. K. Saxena, Phys. Status Solidi B **105**, 777 (1981).
[5] N. Chand, T. Henderson, J. Klem, T. Masselink, R. Fischer, Y. C. Chang, and H. Morkoç, Phys. Rev. B **30**, 4481 (1984).
[6] K. Yamanaka, S. Naritsuka, M. Mannoh, T. Yuasa, Y. Nomura, M. Mihara, and M. Ishii, J. Vac. Sci. Technol. B **2**, 229 (1984).
[7] P. M. Mooney, R. Fisher, and H. Morkoç, J. Appl. Phys. **57**, 1928 (1984).

[8]M. O. Watanabe, K. Morizuka, M. Mashita, Y. Ashizawa, and Y. Zohta, Jpn. J. Appl. Phys. **23**, L103 (1984).

[9]O. Kumagai, H. Kawai, Y. Mori, and K. Kaneko, Appl. Phys. Lett. **45**, 1322 (1984)

[10]M. Tachikawa, M. Mizuta, and H. Kukimoto, Jpn. J. Appl. Phys. **23**, 1594 (1984).

[11]P. M. Mooney, N. S. Caswell, and S. L. Wright, Mater. Res. Soc. Symp. Proc. **46**, 403 (1985).

[12]P. M. Mooney, N. S. Caswell, and S. L. Wright, J. Appl. Phys. **62**, 4786 (1987).

[13]P. M. Mooney, E. Calleja, and S. L. Wright, in *Semi-Insulating III-V Materials,* edited by H. Kukimoto and S. Miyazawa (Ohmsha, Tokyo, 1986), p. 537.

[14]P. M. Mooney, E. Calleja, S. L. Wright, and M. Heiblum, in *Proceedings of the 14th International Conference on the Physics of Semiconductors,* Vols. 10–12 of *Materials Science Forum,* edited by H. J. Von Bardeleben (Trans. Techn., Zurich, 1986), Pt. 1, p. 417.

[15]D. V. Lang, in *Physics of Semiconductors, 1978,* Inst. Phys. Conf. Ser. No. 43, edited by B. L. H. Wilson (IOP, Bristol, 1979), p. 433.

[16]R. Legros, P. M. Mooney, and S. L. Wright, Phys. Rev. B **35**, 7505 (1987).

[17]K. L. Kobayashi, U. Uchida, and H. Nakashima, Jpn. J. Appl. Phys. **24**, L928 (1985).

[18]T. N. Morgan, Phys. Rev. B **34**, 2662 (1986).

[19]A. Oshiyama and S. Ohnishi, Phys. Rev. B **33**, 4320 (1986).

[20]H. P. Hjalmarson and T. J. Drummond, Appl. Phys. Lett. **48**, 656 (1985).

[21]J. C. M. Henning and J. P. M. Ansems, Semicond. Sci. Technol. **2**, 1 (1987).

[22]J. C. Henning, Bull. Am. Phys. Soc. **32**, 504 (1987).

[23]J. C. M. Henning and J. P. M. Ansems, Appl. Phys. A **44**, 245 (1978).

[24]L.-Å. Ledebo, in *Semi-Insulating III-V Materials,* Ref. 13, p. 543.

[25]For a review, see R. G. Smith, in *Lasers: A Series of Advances,* edited by A. K. Levine and A. J. DeMaria (Dekker, New York, 1976), pp. 189–307.

[26]H. G. Grimmeiss and L.-Å. Ledebo, J. Appl. Phys. **46**, 2155 (1975).

[27]H. G. Grimmeiss, Annu. Rev. Mater. Sci. **7**, 341 (1977).

[28]Here, $Q_L=\beta_L X$ is the usual dimensionless harmonic-oscillator coordinate obtained from the actual displacement X of the relevant lattice mode. The conversion factor is $\beta_L=(M\omega_L/\hbar)^{1/2}$, and a similar factor, $\beta_0=(M\omega_0/\hbar)^{1/2}$, applies to the lower minimum. Here, M is the mass for vibration in the mode and ω_0 and ω_L are the corresponding frequencies for motion about $Q=0$ and $Q=Q_0$, respectively. These quantities are also related to the effective stiffness coefficients, K_0 and K_L, by $\omega_0^2=K_0/M$ and $\omega_L^2=K_L/M$.

[29]A report on this calculation is in preparation, T. N. Morgan (unpublished).

[30]Similar conclusions for neutral defects have been found by T. N. Morgan, Phys. Rev. B **28**, 7141 (1983).

[31]To simulate the reduction in electron-phonon coupling with increasing localization, the coupling coefficient was reduced at large Q. The potential used for Fig. 7 was $V(Q)=1.73Q/(1+0.04Q)\delta(r)$, where $\delta(r)$ is the one-band δ function. See Ref. 30.

[32]This would be a quasilocal mode, probably resonant with the lattice phonons. To be more realistic, the analysis should be extended to treat coupling to two or more such modes.

[33]K. Huang and A. Rhys, Proc. R. Soc. London, Ser. A **204**, 406 (1950).

[34]I. S. Gradshteyn and I. M. Ryzhik, *Table of Integrals, Series and Products,* 4th ed. (Academic, New York, 1965), Eq. 3.462.